Available online at www.sciencedirect.com
ScienceDirect
Energy Procedia 1 (2009) 3485–3492
Energy Procedia
www.elsevier.com/locate/procedia

GHGT-9

The mechanical behavior of anhydrite and the effect of CO_2 injection

Suzanne Hangx*, Christopher Spiers, Colin Peach

High Pressure and Temperature Laboratory, Utrecht University, Budapestlaan 4, P.O. Box 80021, 3508 TA, Utrecht, The Netherlands

Abstract

Maintaining caprock integrity is important to long-term geological CO_2 storage. Worldwide, many depleted oil and gas reservoirs, and several current injection sites, are capped by anhydrite caprock. We investigated the effect of CO_2 on the mechanical strength of Zechstein anhydrite, which caps many potential CO_2 storage sites in the Netherlands. No short-term chemical effects of CO_2 and pore fluid on the strength of anhydrite were observed. Reaction of bulk anhydrite with CO_2-saturated solution was slow, though the relative fast reaction of fault gouge material (anhydrite + CO_2 + H_2O → carbonates) could affect long-term mechanical behavior and transport properties.

Keywords: anhydrite, failure behaviour, caprock integrity, mechanical strength, CO_2 effect, healing

1. Introduction

Geological storage of CO_2 in depleted oil and gas reservoirs, saline aquifers and coals seams is one of the most promising options of anthropogenic carbon dioxide emissions mitigation [1, 2]. Depleted reservoirs form an attractive option for implementation of CO_2 storage on the short term, especially in countries with a major hydrocarbons production and transportation infrastructure, such as the Netherlands, Norway and the United States. Of great importance to long term geological storage in reservoirs is maintaining seal integrity. Chemical interaction between CO_2 and caprock minerals may affect the mechanical strength and transport properties of the sealing formation, possibly inducing slip along currently sealing faults, or creating pathways, allowing carbon dioxide seepage.

Anhydrite caprock is a widespread sealing formation for many hydrocarbon reservoirs and several current injection sites (e.g. Weyburn Field and Zama Oil Field, Canada), as well as natural CO_2 occurrences. However, very little data is available on the mechanical properties of anhydrite [3, 4], especially on failure strength, fault friction and changes in transport properties at elevated temperature and in the presence of fluids, such as water and CO_2.

This study reports triaxial experiments performed on anhydrite from the Zechstein formation, which caps many potential CO_2 storage sites in the Netherlands. Our aim was to study the effect of CO_2 on the mechanical behavior of anhydrite caprock. Experiments were performed at temperatures of 20-80°C, confining pressures, P_c, of 1.5-50 MPa

* Corresponding author. Tel.: +31 (0)30 253 49 76; fax: +31 (0)30 253 77 25.
E-mail address: hangx@geo.uu.nl.

doi:10.1016/j.egypro.2009.02.140

and relatively rapid strain rates (~ 10^{-5} s^{-1}). We determined the mechanical failure envelope of dry anhydrite and studied the effect upon it of high pressure pore fluids (P_f = 15 MPa) consisting of saturated $CaSO_4$ solution and CO_2-saturated aqueous fluid. Assuming penetration of the pores by the fluid phase and in the absence of any chemical effects, the failure behavior is determined by the effective pressure.

Aside from direct mechanical effects (effective pressure), it is expected that anhydrite will react with supercritical CO_2 and water to form carbonates and this might affect the mechanical behavior. It may be possible that, on a shorter timescale, chemical interaction will affect microcracking processes, as is seen for silicate minerals [5]. On the longer term, reaction could be important in affecting transport properties and in the healing of fractures. Therefore, alongside the triaxial experiments, we also performed batch experiments on coarse and fine grain size fractions of anhydrite, to investigate the reaction of "fault gouge" (25 ± 10 μm) and "bulk" anhydrite (200 ± 50 μm) with water and supercritical CO_2.

2. Experimental methods

2.1. Materials and fluids

The anhydrite rock used in the present experiments was drilled perpendicular to the bedding of the Zechstein formation, near Assen, the Netherlands. Thermogravimetric analysis (TGA) showed that the material contained between 10 and 33 wt% carbonate, most likely dolomite. Porosity varied from 0.1 to 0.3 % and permeability was less than 10^{-22} m^2. The samples displayed a clear bimodal grain size distribution of coarse needle-like anhydrite crystals (~100-200 μm) embedded in a very fine grained matrix (1-5 μm). For the batch experiments, two grain size fractions (25 ± 10 μm and 200 ± 50 μm) were prepared by grounding, using a mortar and pestle, sieving and gravitational settling in water. Saturated anhydrite solution was prepared by dissolution of an excess of ground sample material (> 2.72 g/l [6]) into distilled water under continuous stirring for two days.

2.2. Experimental set-ups

Triaxial compression experiments were performed using a triaxial deformation apparatus. The current apparatus is a modified version of the triaxial machine described extensively by Peach [7] and Peach and Spiers [8]. The main modifications made to the apparatus include changing the sample size (∅ = 35 mm, L = 75 mm) and connecting part of the existing pore fluid system to a CO_2 pump (ISCO 65D). Throughout the experiments, axial internal load, piston displacement, confining pressure, sample temperature, pore fluid pressure, pore fluid volume change, CO_2 pressure, and CO_2 volume change are measured. The raw data are processed to yield effective axial stress and axial strain as functions of time. The displacement data required correction for apparatus distortion.

Batch experiments were performed using a cold seal pressure vessel. The method and experimental set-up are described by Hangx and Spiers [9]. Experiments were performed under reservoir conditions (80°C, 10 MPa $P(CO_2)$) in the presence of CO_2-saturated pore fluid.

Table 1. Compilation of the mechanical data of the compression experiments on dry anhydrite at 20 and 80°C

sample	P_c [MPa]	$(\sigma_1 - \sigma_3)_{max}$ [MPa]	σ_Y [MPa]
Dry anhydrite, 20°C			
HBG-7	1.5	97.7	93.4
HBG-9	3.0	129.2	124.2
HBG-4	5.0	149.3	145.0
HBG-6	10.0	173.5	156.4
HBG-5	15.0	167.4	156.0
HBG-49	25.0	195.6	172.7
HBG-48	50.0	232.5	189.8
Dry anhydrite, 80°C			
HBG-18	1.5	121.3	117.0
HBG-17	3.0	137.6	130.5
HBG-12	5.0	127.9	121.0
HBG-8	10.0	140.0	123.8
HBG-10	15.0	168.5	146.8
HBG-13	25.0	180.5	159.9
HBG14	35.0	197.9	173.4
HBG-15	50.0	222.2	185.1

3. Results

In this paper, we have adopted the convention that compressive stresses and compressive axial strains are positive. The principle

stresses are denoted σ_i, with $\sigma_1 > \sigma_2 = \sigma_3$, where σ_3 is the confining pressure (P_c). A list of experiments and mechanical data obtained for anhydrite deformed at 20 and 80°C, under dry and wet conditions, is shown in Tables 1 and 2.

3.1. Dry experiments at room temperature

Axial stress-strain curves for experiments performed on dry anhydrite, deformed at room temperature at confining pressures in the range 1.5 to 50 MPa, are shown in Figure 1.

Up to confining pressures of 5 MPa, the stress-strain behavior shows strain softening after attaining the peak differential stress. Samples are characterized by brittle failure along a single macroscopic shear fracture. Brittle failure is accompanied by audible acoustic emission and the failure plane is orientated at approximately 30° with respect to the σ_1 direction.

In the confining pressure range 10 to 50 MPa, the stress-strain curves (Fig. 1) indicate a transient stage of strain-softening after the peak differential stress is reached. Samples display semi-brittle behavior, showing a network of shear fractures together with a slight shear displacement along one macroscopic fracture, without loss of cohesion. No barreling of the samples was observed.

Overall, peak differential stress ($(\sigma_1 - \sigma_3)_{max}$) increases with confining pressure. A similar correlation with P_c is observed for the yield stress (σ_y), defined as the differential stress at which the axial stress-strain curve deviates from linearity (see Table 1 and Fig. 1).

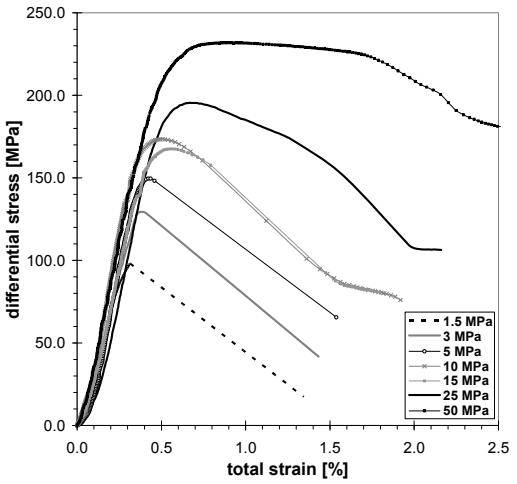

Fig. 1 Axial stress-strain curves for triaxial experiments performed on dry anhydrite at 20°C. Confining pressure ranged from 1.5 to 50 MPa

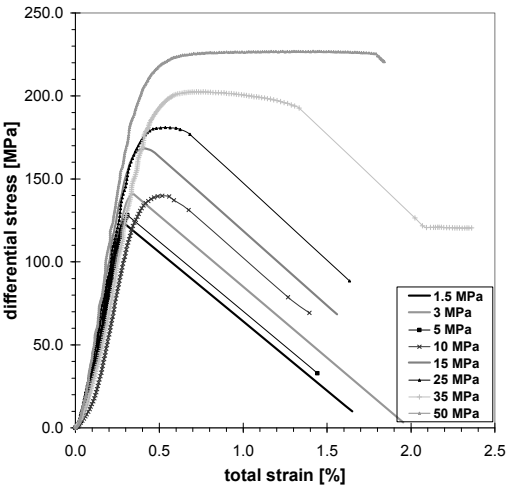

Fig. 2 Axial stress-strain curves for triaxial experiments performed on dry anhydrite at 80°C. Confining pressure ranged from 1.5 to 50 MPa

3.2. Dry experiments at 80°C

Axial stress-strain behavior for experiments performed at 80°C and confining pressures of 1.5 to 50 MPa is plotted in Figure 2.

The behavior of dry anhydrite at higher temperature (80°C) is similar to that observed at room temperature. At 80°C, the brittle regime extends up to 15 MPa confining pressure. After attaining the peak differential stress strain softening is observed, this is accompanied by audible acoustic emissions. Samples display failure along a single macroscopic fracture (orientation to σ_1 direction: ~30°).

Semi-brittle behavior is observed in the range of 25 to 50 MPa confining pressure, showing a transient stage of strain-softening after attaining peak stress. Sample HBG-13, deformed at 25 MPa confining pressure, failed across a single macroscopic shear fracture, which is surrounded by a network of shear oriented cracks. In contrast, samples deformed at higher confining pressure show multiple shear fractures plus minor displacement along a single fracture, without loss of cohesion. Similar to the room temperature experiments, samples showed no barreling.

Over the confining pressure range (1.5-50 MPa), there is a positive correlation with both the peak differential stress $(\sigma_1 - \sigma_3)_{max}$ and yield stress σ_y, as seen in Table 1 and Figure 2.

3.3. Wet experiments - $CaSO_4$-saturated solution

Two sets of experiments were performed on anhydrite in contact with $CaSO_4$-saturated solution (P_c = 25 MPa, P_f = 15 MPa): 1) on intact samples; and 2) on samples that underwent a deformation cycle up to 85% of their full strength (P_c = 10 MPa) , prior to fluid injection. Axial stress-strain curves for the experiments performed at room temperature and 80°C are shown in Figure 3. For comparison the stress-strain curves for dry samples deformed at 10 and 25 MPa confining pressure are added. A list of experiments and mechanical data is shown in Table 2.

At room temperature, the intact sample initially behaves similarly to dry samples deformed at 25 MPa P_c. At the point where the sample is deformed up to 80% of its compressive strength, fluid penetration is observed and the sample shows behavior comparable to that of dry samples deformed at 10 MPa P_c. Failure occurred along a conjugate set of shear fractures. The pre-deformed sample showed premature failure during the unloading stage of the first deformation cycle. Therefore, the effect of aqueous solution can not be assessed for this sample.

The experiments performed at 80°C show no penetration of aqueous fluid in the intact or pre-deformed samples, until failure occurs. Prior to failure both samples behave similarly to dry samples deformed at 25 MPa confining pressure. Samples HBG-20 and -21 display multiple shear fractures and brittle failure along a conjugate set of macroscopic shear fractures.

Table 2. Compilation of the mechanical data of the compression experiments on water-wet and CO_2-wet anhydrite at 20 and 80°C

sample	T [°C]	P_c [MPa]	$(\sigma_1 - \sigma_3)_{max}$ [MPa]
Wet anhydrite ($CaSO_4$-saturated solution)			
HBG-16	20	25.0	174.6
HBG-20*	80	10.0	133.2
		25.0	177.1
HBG-21	80	25.0	187.8
CO_2-wet anhydrite (CO_2-saturated solution)			
HBG-37*	20	10.0	129.4
		25.0	170.7
HBG-46	20	25.0	158.7
HBG-40*	80	10.0	119.3
		25.0	149.9
HBG-42	80	25.0	153.8

* pre-deformed sample; initial deformation cycle up to ~85% of the compressive strength

3.4. Experiments using CO_2-saturated solution

For the samples in contact with CO_2-saturated solution the same procedure was used as for the $CaSO_4$-saturated solution experiments (see Section 3.3). Figure 4 displays the axial stress-strain data for both 20 and 80°C experiments and plots for dry anhydrite deformed at 10 and 25 MPa confining pressure are added for comparison. Table 2 contains a compilation of mechanical data of these experiments.

All samples behave similarly to dry samples deformed at 10 MPa confining pressure, as can be seen in Figure 4. No significant fluid inflow was observed until after failure. The samples show multiple shear oriented fractures near the shear planes and shear failure occurred along a conjugate set of fractures. In addition, samples HBG-40 and -42, deformed at higher temperature (80°C), show a yellowish discoloration.

3.5. Batch reaction experiments

Thermogravimetric analysis on anhydrite, reacted with supercritical CO_2 under reservoir conditions (80°C, 10 MPa CO_2 pressure) for one week, indicate that the carbonate content of fine grained anhydrite (simulating fault

gouge, 25 ± 10 μm) increased by 15 wt%. In comparison, coarse grained anhydrite (simulating bulk material, 200 ± 50 μm) shows no difference in carbonate content.

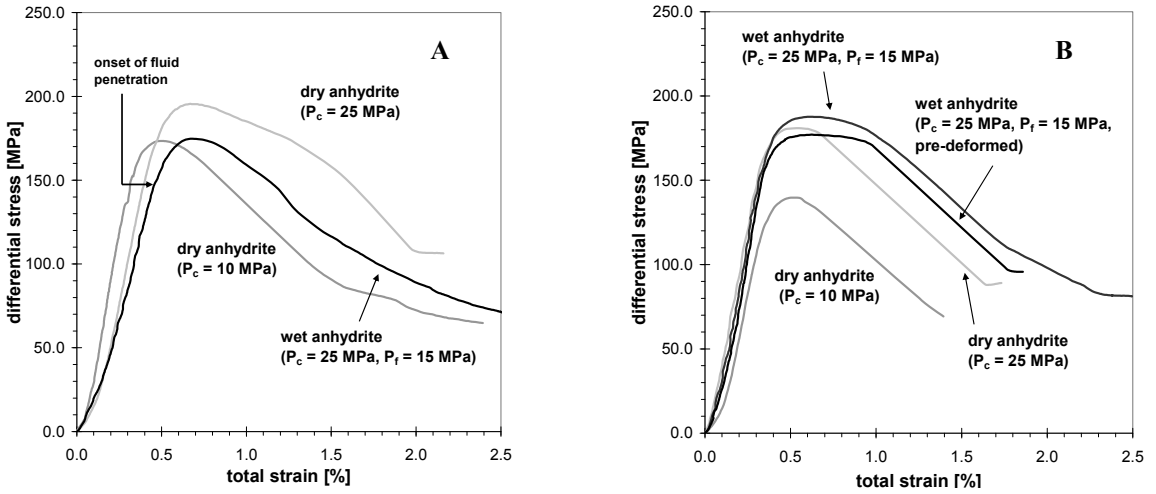

Fig. 3 Axial stress-strain curves for triaxial experiments performed on wet anhydrite ($CaSO_4$-saturated solution) at P_c = 25 MPa and P_f = 15 MPa. For comparison the curves for dry anhydrite, deformed at 10 and 25 MPa confining pressure, were added. Experiments are performed at A) 20°C, and B) 80°C.

4. Discussion

4.1. Failure under dry conditions

Under the experimental range of confining pressures (1.5-50 MPa) and temperatures of 20-80°C, samples evolved from macroscopically brittle to more cataclastic flow-like, semi-brittle behavior with increasing confining pressure. No true ductile behavior of anhydrite was observed. In the semi-brittle regime, macroscopically shear fractures were formed but no loss of cohesion was observed, most likely due to compaction of the fault gouge under high confining pressures. Some weakening was observed by the increase in temperature, with the most pronounced effect being the shift of the brittle/semi-brittle transition to higher confining pressure.

We plotted our data in the (τ_{oct}, $\sigma_{m,2}$) plane of the Mogi failure criterion [10] (Fig. 5). The Mogi failure criterion was chosen over the more conventional Coulomb criterion, as the former gives a better linear fit to our data. Generally the Mogi failure criterion is used to describe the results of true triaxial (polyaxial) compression experiments, as it takes into account the effect of the intermediate stress σ_2. It has been proven [11] that the Mogi criterion can also be used to accurately describe data from conventional triaxial tests. The stress space of the Mogi failure criterion is described by the octahedral shear stress τ_{oct} and the mean stress $\sigma_{m,2}$. In the case where $\sigma_2 = \sigma_3$, such as for our experiments, the criterion is reduced to $\tau_{oct} = \sqrt{2}/3\ (\sigma_1 - \sigma_3)$ and $\sigma_{m,2} = (\sigma_1 + \sigma_3)/2$.

Our failure envelopes for dry anhydrite deformed at 20 and 80°C can be described by linear trends, given as

$$\text{at } 20°C: \tau_{oct} = 25.292 + 0.5321\sigma_{m,2},\ R^2 = 0.9665 \quad (1)$$

$$\text{at } 80°C: \tau_{oct} = 28.592 + 0.4825\sigma_{m,2},\ R^2 = 0.9900 \quad (2)$$

As suggested by Al-Ajmi and Zimmerman [11], the linear trends observed in the Mogi stress space can be translated to a linear Coulomb criterion. We rewrote the linear expressions obtained from the Mogi failure criterion in the form of the Coulomb failure parameters C_0 (uniaxial compressive strength) and θ (angle of the fracture plane

with respect to σ_3), describing the linear Coulomb criterion $\sigma_1 = C_0 + \tan^2\theta\ \sigma_3$. This resulted in the following equations

$$\text{at } 20°C: \sigma_1 = 123.16 + 3.59\sigma_3 \quad (3)$$
$$\text{at } 80°C: \sigma_1 = 124.23 + 3.09\sigma_3 \quad (4)$$

In addition to the failure parameters, we used the linear part of the loading curves to estimate the Young's Modulus from the stress-strain data of our dry anhydrite samples. At room temperature, the Young's Modulus is 39.7 ± 9.2 GPa, while at 80°C it's 49.4 ± 7.9 GPa. No systematic variation of Young's Modulus with increasing confining pressure was observed.

Comparison with other studies shows that our data are comparable to the results of Müller and Siemes [4]. They also performed compression experiments on Zechstein anhydrite, at temperatures up to 300°C and confining pressures up to 500 MPa. They observed brittle behavior up to 100 MPa at room temperature and a decrease is strength with increasing temperature, at low axial strains (< 5%). We also compared our data with the results obtained by Liang et al. [3] on anhydrite obtained from the Yingcheng salt deposit (China) at room temperature and 5 to 15 MPa confining pressure. The mechanical strength of Zechstein anhydrite is a factor of ~2 higher than that of Yingcheng anhydrite. Over the range of confining pressures, Liang et al. [3] also observed brittle behavior, though through the formation of axial extensional fractures.

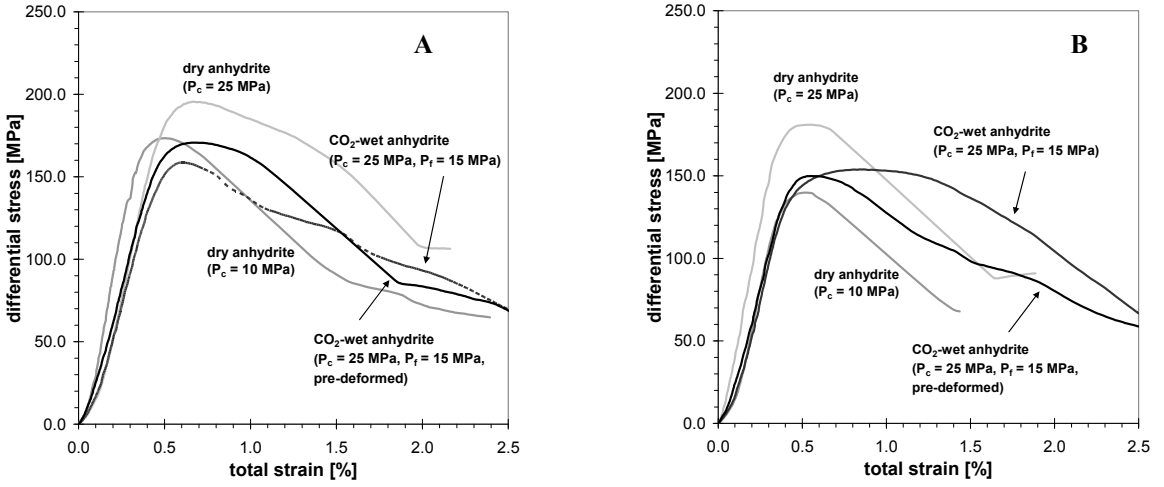

Fig. 4 Axial stress-strain curves for triaxial experiments performed on CO_2-wet anhydrite (CO_2-saturated solution) at P_c = 25 MPa and P_f = 15 MPa. For comparison, the curves for dry anhydrite, deformed at 10 and 25 MPa confining pressure, were added. Experiments are performed at A) 20°C, and B) 80°C.

4.2. Failure under wet conditions – saturated $CaSO_4$ solution

In case of fluid penetrating the pores of a material, the pressure working in the material is modified to yield an effective pressure, given as $\sigma_i^{eff} = \sigma_i - P_f$, where, σ_i^{eff} is the effective principle stress, σ_i is the principle stress, P_f is the pore fluid pressure, and *i* has a value between 1 and 3, denoting the principle stress direction. During the room temperature water-wet experiments on intact samples (HBG-16), a stage of fluid flow was observed when approximately 80% of the maximum material strength was reached, leading to a transient change in stress regime. Therefore, the sample initially behaved similar to dry anhydrite deformed at 25 MPa effective P_c, and gradually started to behave as dry anhydrite deformed at 10 MPa effective P_c, as fluid penetrated the sample. Besides the change in effective pressure, no additional chemical effect of the $CaSO_4$-saturated solution on the mechanical strength of anhydrite was observed on the timescale of the experiments (~5h).

At higher temperature (80°C), no fluid penetration was observed, indicating that the samples (intact and pre-deformed) did not become permeable during the experiment. Samples behaved similarly to dry anhydrite deformed at 25 MPa effective confining pressure.

4.3. Failure behavior in the presence of supercritical CO_2 and aqueous solution

At both 20 and 80°C, no significant CO_2 inflow was observed during the experiments, until failure occurred, and both intact and pre-deformed samples behave similarly to dry anhydrite deformed at 10 MPa effective confining pressure. This indicates that, prior to deformation, the CO_2-saturated solution had penetrated the samples, putting constraints on the entry pressure of our material (i.e. capillary entry pressure, $P_{ce} < 15$ MPa). Breakthrough pressure experiments on anhydrite of the Weyburn field [12] showed that the maximum breakthrough pressure for the Weyburn Midale Evaporite caprock ($\varphi \sim 0.5$ %, $\kappa \sim 10^{-20}$ m^2) is in the range 9 to 21 MPa P(CO_2). The interfacial tension of the CO_2/water system [12] is significantly lower than of the air/water system [13], which could explain the penetration of the samples by CO_2-saturated solution but not by water. No significant effect of CO_2 on the mechanical strength of anhydrite was observed on the timescale of the experiments (~5h).

5. Implications for caprock integrity

CO_2 injection into depleted gas and oil reservoirs changes the stress state of the system, which may lead to failure of the caprock. Our data show that on very short time scales there is no chemical effect of pore fluid, with or without CO_2, on the strength of anhydrite. This is in contrast to effects observed for other reservoir rocks, such as sandstones, which show a significant weakening by the addition of water [5]. Baud et al. [5] inferred that this weakening was the result of enhanced microcracking. Following the same reasoning, it is likely that in our experiments the added pore fluids do not significantly lower the surface free energy or induce subcritical microcracking in anhydrite. It should be noted though that the breakthrough pressure of the caprock has to be taken into account, as the sealing capacity of a caprock is provided by the capillary forced across the interface of the wetting phase (brine) and the nonwetting phase (CO_2) [12]. The entry pressure of Zechstein anhydrite is 15 MPa or less, as indicated by our experiments. Furthermore, our results can be used together with finite element modeling to predict caprock response to changing stress states, as a result of fluid injection or depletion.

Reaction experiments on fine and coarse grained anhydrite plus water and supercritical CO_2 show that reaction of fine "fault gouge-like" material is fairly rapid, resulting in a substantial increase (15 wt%) in carbonate content within one week. On the other hand, reaction of coarse "bulk-like" material with water and CO_2 is slow on this timescale. These results indicate that reaction between anhydrite and CO_2-saturated solutions may affect mechanical behavior and transport properties on the long-term and could possibly results in healing of fractures formed at the base of the caprock, as a result of doming, in response to poroelastic expansion of the reservoir rock.

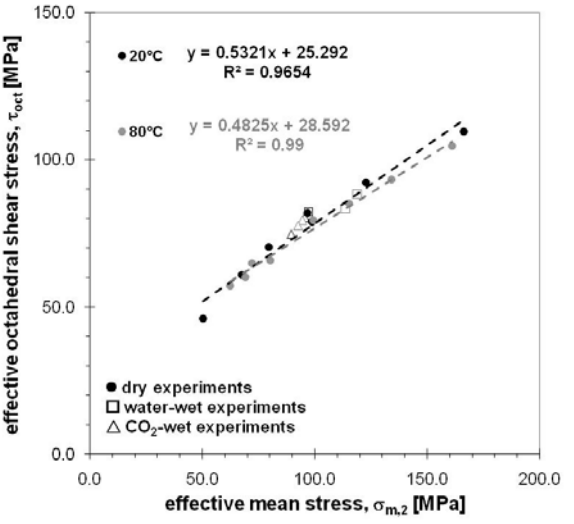

Fig. 5 Linear Mogi criteria for dry failure of anhydrite, at 20 (black) to 80°C (grey) and 1.5 to 50 MPa confining pressure. Wet anhydrite data are indicated by □, and CO_2-wet anhydrite data by Δ.

6. Conclusions

We have investigated the effect of CO_2 on the mechanical strength of anhydrite. To this end, we performed triaxial compression experiments on anhydrite, under dry, water-wet and CO_2-wet conditions at 20 and

80°C at confining pressures of 1.5 to 50 MPa. Our main findings can be summarized as:

1. In the confining pressure range of 1.5 to 50 MPa, a transition from brittle to semi-brittle behavior was observed. At room temperature this transition occurred at 5 to 10 MPa confining pressure. At higher temperature (80°C) the transition moved to higher confining pressure, 15 to 25 MPa. A slight weakening of the material was observed as a result of increasing temperature.
2. The failure behavior of Zechstein anhydrite can be described by the Mogi criterion. At 20°C the criterion yields $\tau_{oct} = 25.292 + 0.5321\sigma_{m,2}$, and at 80°C it is given as $\tau_{oct} = 28.592 + 0.4825\sigma_{m,2}$.
3. On the timescale of the experiments (~5h) no chemical effects of $CaSO_4$-saturated solution and CO_2-saturated aqueous fluid on the mechanical strength of anhydrite was observed.
4. The mechanical data obtained for Zechstein anhydrite can be used together with finite element modelling to predict caprock response to changing stress states, as a result of CO_2 injection.
5. Reaction of bulk anhydrite with CO_2 and pore fluid is slow, though on the long-term mechanical behavior and transport properties could be affected. Fault gouge appears to react relatively rapid with CO_2-saturated fluids, which could result in healing of fractures developing at the base of the caprock.

Acknowledgements

This research was funded by Shell International Exploration and Production and performed within WorkPackage 4.1 Subsurface mineralisation of the Dutch national research project CATO, CO_2 capture, transport and storage. We thank Eimert de Graaff, Gert Kastelein, and Peter van Krieken for technical assistance.

References

[1] Bachu, S., Sequestration of CO_2 in geological media: criteria and approach for site selection in response to climate change, Energy Convers. Manage. 41 (2000) 953-970.
[2] Orr Jr., F. M., Storage of carbon dioxide in geologic formations, J. Petrol. Technol. 56 (2004) 90-97.
[3] Liang, W., C. Yang, Y. Zhao, M. B. Dusseault and J. Liu, Experimental investigation of mechanical properties of bedded salt rock, Int. J. Rock Mech. Sci. Geomech. 44 (2007) 400-411.
[4] Müller, P. and H. Siemes, Festigkeit, verformbarkeit und gefügeregelung von anhydrit -- experimentelle stauchverformung unter manteldrucken bis 5 kbar bei temperaturen bis 300°C, Tectonophysics 23 (1974) 105-127.
[5] Baud, P., W. Zhu and T.-F. Wong, Failure mode and weakening effect of water on sandstone, J. Geophys. Res. 105 (2000) 16371-16389.
[6] Kontrec, J., D. Kralj and L. Brecevic, Transformation of anhydrous calcium sulphate into calcium sulphate dihydrate in aqueous solutions, J. Cryst. Growth 240 (2002) 203-211.
[7] Peach, C. J., Influence of deformation on the fluid transport properties of salt rocks. In: Faculty of Geosciences, Utrecht University, Utrecht, (1991) pp. 238.
[8] Peach, C. J. and C. J. Spiers, Influence of crystal plastic deformation on dilatancy and permeability development in synthetic salt rock, Tectonophysics 256 (1996) 101-128.
[9] Hangx, S. J. T. and C. J. Spiers, Reaction of plagioclase feldspar with CO_2 under hydrothermal conditions (submitted to Chemical Geology)
[10] Mogi, K., Fracture and flow of rocks under high triaxial compression, J. Geophys. Res. 76 (1971) 1255-1269.
[11] Al-Ajmi, A. M. and R. W. Zimmerman, Relation between the Mogi and the Coulomb failure criteria, Int. J. Rock Mech. Sci. Geomech. 42 (2005) 431-439.
[12] Li, S., M. Dong, Z. Li, S. Huang, H. Qing and E. Nickel, Gas breakthrough pressure for hydrocarbon reservoir seal rocks: implications for the security of long-term CO_2 storage in the Weyburn field, Geofluids 5 (2005) 326-334.
[13] Pallas, N. R. and B. A. Pethica, The surface tension of water, Colloids and Surfaces 6 (1983) 221-227.